M. Rad, H. Nishikawa and P. L. Roe ,
Some Properties of Residual Distribution Schemes for Euler Equations,
Computational Fluid Dynamics 2000: Proceedings of the First International Conference on Computational Fluid Dynamics, ICCFD, Kyoto, Japan, 10-14 July 2000, Springer, 2001.

Some Properties of Residual Distribution Schemes for the Euler Equations

Mani Rad, Hiroaki Nishikawa, and Philip L. Roe

University of Michigan, Ann Arbor MI 48105, USA

Abstract. A residual distribution technique is presented for the Euler equations, one which splits the updates into purely elliptic and hyperbolic contributions. The scheme combines fluctuation splitting methods ideal for scalar advection and a least squares minimisation appropriate for the elliptic subsystem. The minimisation is constrained to maximally decouple effects of the entropy, enthalpy and acoustic parts from each other. Results show that for subcritical flows where potential solutions should be obtained, the enthalpy is constant to machine zero, and the entropy is constant to an extremely high degree of accuracy. Still under investigation, fluctuation calculations with dissipative effects are presented. They are capable of breaking rarefaction shocks for fluctuation splitting schemes in grid-aligned cases.

1 Introduction

Fluctuation splitting (FS) schemes for Euler and other equations that share similar structure have made it well in their way into the literature. As in past efforts, the present work takes a physical approach to strongly discontinuous flows while avoiding the defects of upwind methods applied to almost incompressible flow. Using the decomposed form of the Euler equations together with a residual distribution scheme provides the advantage that the elliptic and hyperbolic parts of the problems are handled separately, with maximal decoupling. To illustrate the scheme's accuracy and test its properties, we choose a set of flow problems containing difficult features to capture. Further robustness study reveals that FS is not immune to grid dependency and in combination with certain choices of meshes will produce non-physical solutions.

2 Uniquely Decomposed Form of the Euler Equations

Different properties of the Euler equations are emphasized by proper selection of the set of unknowns. For computing compressible flow, the most fundamental choice is the set of *conserved quantities* $\mathbf{u} = (\rho, \rho\mathbf{v}, \rho E)^t$ associated with the flux tensor $\underline{\underline{\mathbf{F}}} = (\rho\mathbf{v}, \rho\mathbf{v} \otimes \mathbf{v} + p\underline{\underline{\mathbf{I}}}, \mathbf{v}(E+p))^t$ since they satisfy the Rankine-Hugoniot conditions across discontinuities.

For computational convenience we use another set of unknowns, the *parameter vector* $\mathbf{z} = \sqrt{\rho}(1, \mathbf{v}, h)^t$, where h is the total specific enthalpy. This set allows the construction of local linearizations having conservation properties [1] [6]. Furthermore, of significance to the present approach, are the *natural variables* [3].

They are written as $\mathbf{x} = (S, h, p, \mathbf{v}/|\mathbf{v}|)^t$ and $\mathbf{x} = (S, h, W^+, W^-)^t$ respectively in subsonic and supersonic flow. In the supersonic regime, the acoustic Riemann invariants are $\partial W^+ = \beta\partial p + \rho q^2 \partial\theta$, $\partial W^- = \beta\partial p - \rho q^2\partial\theta$. It is uniquely in these variables that the Euler equations can be decoupled into maximally independent subsystems [3] [7] [9]. These variables enable the inherently different hyperbolic and elliptic behaviour to be computed independently with the minimum of "crosstalk". The decomposed form of the Euler equations can generically be written as $\hat{A}\mathbf{x}_s + \hat{B}\mathbf{x}_n = 0$ or more precisely as follows.

$$\begin{array}{ll} (1-M^2)\partial_s p - \rho q^2 \partial_n \theta = 0 & (\beta\partial_s + \partial_n)W^+ = 0 \\ \rho q^2 \partial_s \theta + \partial_n p = 0 & (\beta\partial_s - \partial_n)W^- = 0 \\ \partial_s S = 0 & \partial_s S = 0 \\ \partial_s h = 0 & \partial_s h = 0 \end{array} \tag{1}$$

3 Advection of Entropy, Enthalpy and Acoustic Invariants

Throughout this paper, the term 'update matrix' will reappear frequently because it is a convenient way to think about FS schemes. Let the twelve scalar quantities $\mathbf{W}^n = (\mathbf{w}_a, \mathbf{w}_b, \mathbf{w}_c)$ represent the initial state of a cell (in two dimensions) with vertices (a,b,c) and $\mathbf{w}$ be the quantity stored at the vertices. The update matrix is the constant matrix within the cell that defines the update $\mathbf{W}^{n+1} - \mathbf{W}^n = \omega U \mathbf{W}^n$. Among its nine blocks, $U_{i,j}$ would be the (i,j) block of the update matrix, signifying the effect of vertex i on j $(i,j = a,b,c)$.

As shown in (1), the Euler equations always exhibit a hyperbolic behaviour through entropy and enthalpy (S&h) advection. In supersonic regime, this behaviour is extended to the acoustic part. Through a rotation transformation, (1) becomes $\tilde{A}\mathbf{x}_x + \tilde{B}\mathbf{x}_y = 0$ where $\tilde{A} = \mathrm{diag}(u, u, u\beta - v, v\beta + u)$ and $\tilde{B} = \mathrm{diag}(v, v, u\beta + v, v\beta - u)$. The fluctuation then becomes

$$\Phi = \frac{1}{A^T} \sum_{j=a,b,c} \mathcal{D}\left(\tilde{A}\Delta y_j - \tilde{B}\Delta x_j\right) \frac{\partial \mathbf{x}}{\partial \mathbf{z}} \mathbf{z_j}$$

The acoustic part of the fluctuation is split apart from the S&h part using respectively the diagonal matrices $\mathcal{D} = \mathrm{diag}(0,0,1,1)$ and $\mathcal{D} = \mathrm{diag}(1,1,0,0)$. This splitting becomes important in the subsonic regime where the S&h part is treated identically as in the supersonic case. Meanwhile the acoustic part becomes an elliptic subsystem and is handled using a distribution scheme with no directional bias.

The fluctuation is then distributed by the favorite FS scheme having distribution coefficient matrix $\mathbf{\Phi}$. Assuming that we are storing the *parameter vector* $\mathbf{z}$ at the vertices, the (i,j) block of the update matrix becomes

$$U_{i,j} = \frac{1}{A^T} \mathbf{\Phi} \left(\frac{\partial \mathbf{x}}{\partial \mathbf{z}}\right)^{-1} \mathcal{D}\left(\tilde{A}\Delta y_j - \tilde{B}\Delta x_j\right) \frac{\partial \mathbf{x}}{\partial \mathbf{z}}$$

where

$$\frac{\partial \mathbf{x}}{\partial \mathbf{z}} = \begin{bmatrix} \frac{z_1 z_4(1-2\gamma)+\gamma(z_2^2+z_3^2)}{z_1} & -z_2 & -z_3 & z_1 \\ -\frac{z_4}{z_1} & 0 & 0 & 1 \\ \frac{\gamma-1}{\gamma}\beta z_4 & -\frac{\gamma-1}{\gamma}\beta z_2 - z_3 & -\frac{\gamma-1}{\gamma}\beta z_3 + z_2 & \frac{\gamma-1}{\gamma}\beta z_1 \\ \frac{\gamma-1}{\gamma}\beta z_4 & -\frac{\gamma-1}{\gamma}\beta z_2 + z_3 & -\frac{\gamma-1}{\gamma}\beta z_3 - z_2 & \frac{\gamma-1}{\gamma}\beta z_1 \end{bmatrix}$$

4 Treatment of the Elliptic Subsystem

This section briefly describes the solution method for the independant acoustic subsystem in (1). For a more detailed account, refer to [5]. If we choose to store the natural variables $\mathbf{x}$, the four residuals $\phi_{\mathbf{x}}$ in (1) can be written as a linear function of the vertex values

$$\phi_{\mathbf{x}} = \sum_{j=a,b,c} R_j \mathbf{x}_j$$

Since in fact we are storing the parameter vector $\mathbf{z}$ we must estimate the quantity to be minimised as

$$\phi_{\mathbf{z}} = \sum_{j=a,b,c} R_j \frac{\partial \mathbf{x}}{\partial \mathbf{z}} \mathbf{z_j}$$

Standard methods are used to evaluate R_j, the matrix of derivatives frozen during the update. The first two components of this vector comprise the elliptic part of the problem, if $M < 1$, so the norm to be minimized is

$$\mathcal{D} \sum_{j=a,b,c} R_j \frac{\partial \mathbf{x}}{\partial \mathbf{z}} \mathbf{z_j} \quad \text{where} \quad \mathcal{D} = \text{diag}(1, \sqrt{1-M^2}, 0, 0)$$

where the relative weighting of the continuity and vorticity residuals follows from [9]. To converge towards steady-state, we choose a least squares minimisation using a steepest descent method. Steepest descent minimization is selected for illustration purposes only, one would revert to more efficient (mainly Newton-like) methods for any practical Euler code. After determining the gradient of the norm to be minimised, we conclude that the update matrix is given by

$$U = \left(\sum_{j=a,b,c} R_j \frac{\partial \mathbf{x}}{\partial \mathbf{z}} \right)^t \mathcal{D}^2 \left(\sum_{j=a,b,c} R_j \frac{\partial \mathbf{x}}{\partial \mathbf{z}} \right)$$

The update found in this manner has the disadvantage of changing the convected quantities, S&h. Since we intend complete decoupling at the update level between the elliptic and hyperbolic parts, the elliptic part of the residual should only contribute to changes in pressure and flow angle and not to S&h. A necessary step is to perform a constrained minimisation of the elliptic residual. This means that the updates from the elliptic residual should be in directions where only pressure and flow angle change. For the *natural variables*, the direction of a vector along which only that variable changes is $r_S = (\frac{1}{2}\frac{z_2^2+z_3^2}{z_4}, z_2, z_3, \frac{1}{2}\frac{z_2^2+z_3^2}{z_1})^t$, $r_h = (0, z_2, z_3, \frac{z_2^2+z_3^2}{z_1})^t$, $r_p = (\frac{M^2}{M^2-2}z_1, z_2, z_3, \frac{M^2}{M^2-2}z_4)^t$ and $r_\theta = (0, -z_3, z_2, 0)^t$.

5 Entropy Satisfying Solutions

In a study to test the robustness of FS schemes, we found situations where they can produce non-physical solutions. As shown in figure 3, FS is not immune to grid dependency and in combination with certain choices of meshes will produce rarefaction shocks. Figure 3 is a simulation of supersonic flow over a diamond shaped airfoil and a cut across segment AA' will show a jump in pressure as well as an increase in entropy. Confined within a single band of cells, expansion rays do not fan out properly because they are parallel to grid lines. In search of a remedy, our investigation has lead us to focus on the fluctuation calculation rather than a suitable distribution rule. More specifically, for the conservative form of the Euler equations, where the fluxes $\mathbf{F}$, $\mathbf{G}$ are bilinear functions of the parameter vector $\mathbf{z}$, the cell fluctuation can be written as

$$\Phi = \int\int \partial_x \mathbf{F}(\mathbf{z}) + \partial_y \mathbf{G}(\mathbf{z}) = \oint \mathbf{F}(\mathbf{z})dy - \mathbf{G}(\mathbf{z})dx = \oint \mathbf{z}^T \mathbf{C}\mathbf{z}dy - \mathbf{z}^T \mathbf{D}\mathbf{z}dx$$

This leads to an alternative expression for the fluctuation, a formula containing a parameter α which has only a second-order effect on the fluctuation's accuracy.

$$\begin{aligned}\Phi = &\left[\tfrac{\alpha}{2}({\mathbf{z}_1}^T + {\mathbf{z}_3}^T) + (1-\alpha){\mathbf{z}_2}^T\right]\left\{(y_2 - y_1)\mathbf{C} - (x_2 - x_1)\mathbf{D}\right\}(\mathbf{z}_1 - \mathbf{z}_3) + \\ &\left[\tfrac{\alpha}{2}({\mathbf{z}_1}^T + {\mathbf{z}_2}^T) + (1-\alpha){\mathbf{z}_3}^T\right]\left\{(y_3 - y_1)\mathbf{C} - (x_3 - x_1)\mathbf{D}\right\}(\mathbf{z}_1 - \mathbf{z}_2)\end{aligned}$$

Similarly, the above expression can be rearranged in two other ways by permuting the vertex indices. A family of fluctuations is obtained by varying the parameter α and at least three choices reveal interesting properties. For $\alpha = 1$, the fluctuation vanishes when two vertices are in the same state and the edge connecting them is aligned with the local characteristic. Work presented in [4] illustrates how this property is used to capture shocks exactly. For $\alpha = \frac{2}{3}$, one recovers the common method for computing the fluctuation with $\mathbf{z}$ varying linearly along each edge and a single characteristic evaluated at the cell center. Finally, $\alpha = 0$ produces a fluctuation which has nice dissipative effects and breaks up rarefaction shocks. This is illustrated for a scalar example (Burgers equation) in figure 1 where a solution profile free of discontinuities can be obtained for $\alpha = 0$. The extension from the scalar to a system (i.e. Euler) is currently under progress and should eventually lead to entropy-satisfying solutions.

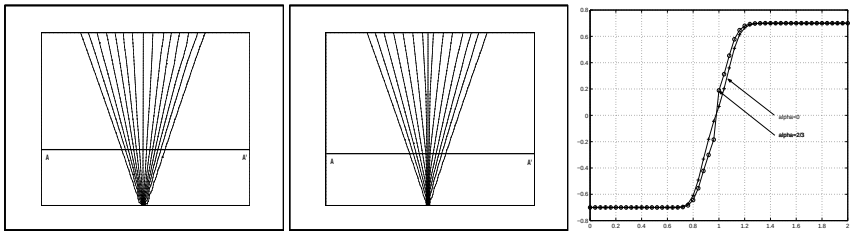

Fig. 1. Rarefaction solution to Burgers equation: $\alpha = 0$, $\alpha = \frac{2}{3}$, cut across AA'

6 Computational Examples and Concluding Remarks

Figure 2 shows computation of subcritical flow around a cylinder at $M_\infty = 0.38$ where constrained least-squared is used for the elliptic part and PSI for the hyperbolic. A potential flow solution should be obtained with perfect fore and aft symmetry. Note the satisfactory behaviour of the solver at stagnation points. Levels of entropy generation were low with $S_{min,max} = -8.5 \times 10^{-6}, 7.3 \times 10^{-6}$.

Figure 3 shows calculations around a supercritical cylinder at $M_\infty = 0.75$ with shock capturing. PSI is used for all advected quantities. The sonic transition is not treated in any special way. Even though the two schemes meeting at $M = 1$ are of very different nature, the solution there is still satisfactory. Note in figure 3, a benign jump in pressure at the sonic line but the levels of entropy are small enough that the discontinuity is neglected

To test the coupling between elliptic and hyperbolic parts, we consider incompressible flow with nonuniform enthalpy at inflow (figure 4). The difficulty in this test case is in exhibiting the recirculation zone which would not be well captured with excessive entropy generation. Convergence tests revealed that our solution approached the exact solution [2] with second order accuracy.

We have illustrated the properties of residual distribution schemes when used in combination with the uniquely decomposed form of the Euler equations. Residual splitting proved appropriate for maximum decoupling between the hyperbolic and elliptic parts. Accurate results are obtained at sonic and stagnation regions, as measured by levels of spurious entropy generation. Still under investigation, new fluctuation calculations with dissipative effects are presented. They are capable of breaking rarefaction shocks for FS schemes in grid-aligned cases.

References

[1] Deconinck, H., Roe, P. L., Struijs, R. J., 'A multidimensional generalisation of Roe's flux difference splitter for the Euler', *Computers and Fluids*, **22**, 1993.

[2] Fraenkel, L. E., 'On Corner Eddies in Plane Inviscid Shear Flow', Journal of Fluid Mechanics, Vol. 11, Part 3, November 1963.

[3] Hayes, W, Probstein, R. F., *Hypersonic Flow Theory*, Academic Press, 1963.

[4] Nishikawa, H., Rad, M., Roe, P. L., 'Grids and Solutions from Residual Minimization', ICCFD Proceedings, Kyoto. Springer-Verlag, 2000.

[5] Rad, M., Roe, P. L., 'An Euler Code that Can Compute Potential Flow', 2nd Inter. Symposium on FV Proceedings, Duisburg. Hermes, 1999

[6] Roe, P. L., 'Approximate Riemann solvers, parameter vectors and difference schemes', *J. Comput. Phys.*, **43**, pp357-372, 1981.

[7] Roe, P. L., Mesaros, L. M., 'Solving steady mixed conservation laws by E/H splitting', 13th Inter. Conf. on Num. Methods in Fl. Dyn., Monterey, July, 1996.

[8] Roe, P. L., Turkel E., 'The quest for diagonalization of differential systems', Workshop on Barriers and Challenges in CFD, NASA Langley 1996. Springer, 1997.

[9] Roe, P. L., 'Compounded of Many Simples, reflection on the role of model problems in CFD', Workshop on Barriers and Challenges in CFD, NASA Langley, August, 1996. Springer, 1997.

[10] Roe, P. L., Rad, M.,'A Form of the Euler Equations Conserving Potential Flow', *AIAA CFD Meeting Proceedings*, Norfolk, VA June, 1999.

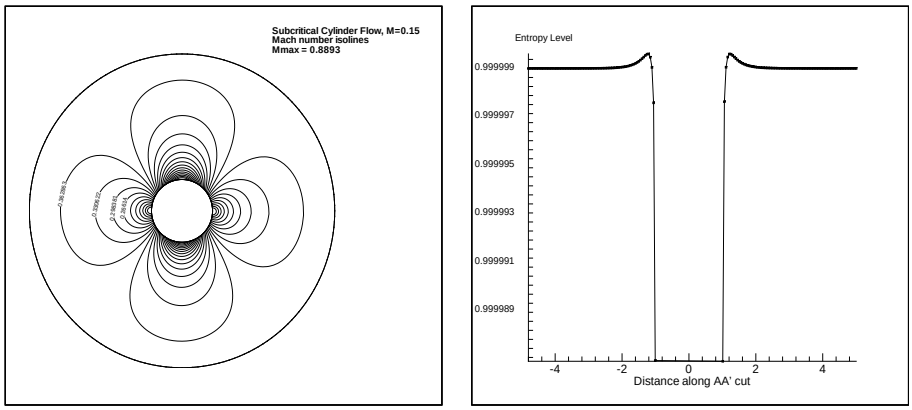

Fig. 2. Subcritical Cylinder Flow at $M_\infty = 0.38$. Mach contours and entropy distributions along vertical cut through center of cylinder

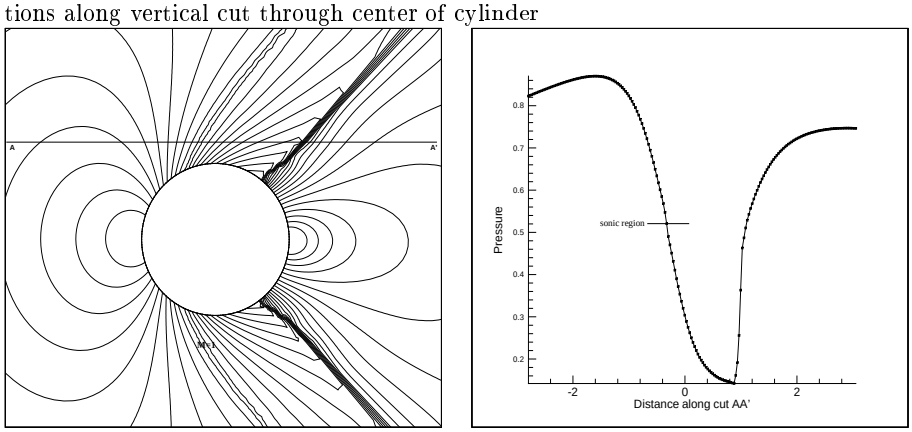

Fig. 3. Supercritical Cylinder Flow at $M_\infty = 0.75$. Mach contours and pressure distributions across AA' cut. Even with no special treatment at the sonic transition, the two separate schemes match well at $M = 1$.

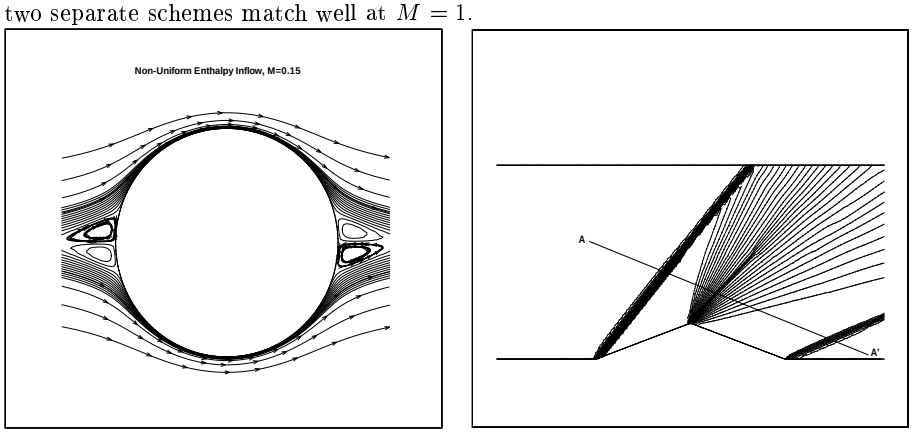

Fig. 4. Non-uniform enthalpy inflow at $M_\infty = 0.15$ showing symmetrical recirculations zones. $M_\infty = 2.0$ flow over a diamond shaped airfoil, showing rarefaction shock.